CALORIMETRY OF THE PALLADIUM - DEUTERIUM SYSTEM

Stanley Pons*
Martin Fleischmann* **

*Department of Chemistry
University of Utah
Salt Lake City UT 84112

**Department of Chemistry
University of Southampton
Southampton, Hants. SO9 5NH
ENGLAND

Abstract

Our calorimetric measurements of the Pd/D system both in the period leading up to the preliminary publication[1] (for some corrections see[2]) and in the period leading up to the submission of the first full paper[3] showed that it is necessary to make measurements on a large number of electrodes for long times (the mean time chosen for a measurement cycle has been 3 months). It has therefore been necessary to adopt a low cost approach; our solution has been to use the single compartment Dewar cell type calorimeters illustrated in Fig.1 and we have maintained up to five of these cells in each of three specially constructed water baths (see Section 1 below). The same type of calorimeter has been used for blank measurements on the Pd-H, Pt-D, and Pt-H systems.

Section 1
Aspects of the Calorimeter and Electrochemical Experiment Design and Calorimetric Measurements

The general principles of the calorimeter design have been outlined elsewhere[3]. The choice of rod electrodes surrounded by a closely wound helical platinum anode allows the axially symmetric injection of heat and, moreover, the uniform charging of the Pd cathodes. Furthermore the choice of such a simple design of calorimeter coupled to the use of rod electrodes allows the iterative adjustment of the dimensions of the systems such that the excess enthalpy to be observed (if any) is large compared to the random errors (see Section 3). The use of a long, thin calorimeter increases the mixing in the calorimeter compared to other possible designs[3]; the minimum current used for most experiments with rod electrodes we have reported to date has been 200mA. Measurements of the mixing history using dye injection (tracer technique of chemical reaction engineering[4]) has shown that radial mixing is extremely rapid (time scale <3s). Axial mixing takes appreciably longer(≅ 20 s) but the axially uniform injection of heat ensures that this longer time scale is unimportant. As the thermal relaxation time is ≅ 1600 s (see Figs. 5A, 6A-C, 7) the cells behave as well stirred tanks. In agreement with this assessment, measurements of the temperature distribution within the cells (using ensembles of 5 thermistors which could be displaced radially and axially) showed that the temperature was uniform to within $\pm 0.01^{\circ}$ throughout the bulk of the cells; this variation rose to $\pm 0.02^{\circ}$ in contact with the Kel-F plugs at the bottom of the cells (all temperature measurements reported here have been made with specially calibrated thermistors (Thermometrics Ultrastable Thermoprobes, ≅ 10 kΩ, ±0.02% stability per year)). Statements which have been made (e.g.[5]) about large temperature fluctuations in cells of this type are incorrect (for a further comment see [6])

All connections to the electrodes were covered in glass and special care has always been taken to ensure that the palladium cathodes and platinum anodes remained totally immersed throughout all of the measurement cycles. In consequence there was no recombination in the gas head spaces (assertions such as those in [7] are incorrect). Furthermore the volumes of gas evolved from the cells corresponded to that from Faraday's law to better than 99% for electrolysis times from approximately 5 diffusional relaxation times to times corresponding to the termination of the experiments (≅ 7 to 200 diffusional relaxation times), and the

records of D_2O additions also matched that predicted for a 100% efficient process for experiments where the cell temperature was within 20° of the bath temperature (30°C). This somewhat surprising result, which has now also been noted in other work,[8,9] can be understood in terms of the inhibition of D_2 ionization at the anode by platinum oxide formation and by degassing of the electrolyte in the vicinity of the cathode by the rapidly evolving D_2 bubbles. This high current efficiency for gas formation greatly simplifies the analysis of the experimental data (see Section 2).

The cells were maintained in specially constructed thermostats (1/2" thick Plexiglas bath surrounded on 5 sides by 2" thick foam insulation bonded on both sides to aluminum foil, the whole structure being enclosed in a 1/16" thick sheet steel container); the water/air interface was allowed to evaporate freely. Stirring with oversized stirrer-temperature regulators ensured that the bath temperature could be controlled to ±0.01° of the set temperature (in the vicinity of 303.15K) throughout the whole space at depths greater than 0.5 cm below the water surface and to ± 0.003° at any given point. The water level in the thermostats was controlled using dosimeter pumps connected to a second thermostat.

All experiments were carried out galvanostatically (Hi-Tek DT2101 potentiostats connected as galvanostats as shown in Fig. 2A). The stability of the systems was monitored oscillographically; the ripple content was <0.04%. For work at current levels outside the operating range of the potentiostats, the circuit shown in Fig. 2B was used (which takes full advantage of the regulation achievable by the potentiostat used as a galvanostat). The systems could be calibrated at any given operating point by using metal film resistor chains in the cells (Digikey ±1% accuracy 5 x 20Ω). The procedure adopted was as follows: after the addition of D_2O (or of electrolyte following sampling for analysis for tritium or HDO) the system was allowed to equilibrate for at least 6 thermal relaxation times. A constant current was then applied to the resistor chain (again supplied by a potentiostat connected as a galvanostat) for 3 hours (i.e. > 6 thermal relaxation times) to give a temperature rise of ≅ 2° above the sloping base line; the current to the calibration system was then switched off and the relaxation of the system to the original base line was followed. Cell parameters and the bath temperature were monitored every 5 minutes using Keithley Model 199 DMM multiplexers to input data to Compaq 386 16MHz computers. The measuring circuits were maintained open except during the actual sampling periods (voltage measurements were allowed to stabilize for 2s before sampling and thermistor resistances 8s before sampling). Data were displayed in real time as well as being written to disks. Fig. 3 illustrates a typical experiment lay-out.

Experiments have been carried out on 0.1, 0.2, 0.4, and 0.8 cm diameter x 10 cm long Pd cathodes (special grade, Johnson Matthey) and on 0.1 x 10 cm Pt electrodes (Johnson Matthey). At the highest current densities used the electrode lengths were reduced to 1.25 cm and the spacings of the anode windings were also reduced. These shorter electrodes were placed at the bottom of the Dewar cells so as to ensure adequate mixing. Measurements reported here were made in D_2O (Cambridge Isotopes) of 99.9% isotopic purity; light water levels were monitored by NMR and never rose above 0.5%. Results reported here have been obtained in 0.1M LiOD prepared by adding Li metal ($^6Li/^7Li$ = 1/9) to D_2O; 0.1M LiOD + 0.1M Li_2SO_4 and 1M Li_2SO_4 were prepared by adding dried Li_2SO_4 (Aldrich 99.99% anhydrous, $^6Li/^7Li$ = 1/11) to 0.1M LiOD and D_2O respectively. A single batch of electrolyte was used for any given experimental series. Blank experiments were carried out using Pd cathodes in 0.1M LiOD in D_2O and Pt cathodes in both in 0.1M LiOD in D_2O and 0.1M LiOH in H_2O.

Section 2
The "Black Box" Representation of the Calorimeters

Data evaluation from the behavior of the Dewar-type electrochemical calorimeters requires the construction of adequately accurate "black-box" models such as that shown in Fig. 4A. In this particular case the models must account for the enthalpy and mass balances in the cell which can be combined through the current efficiency, γ, of the

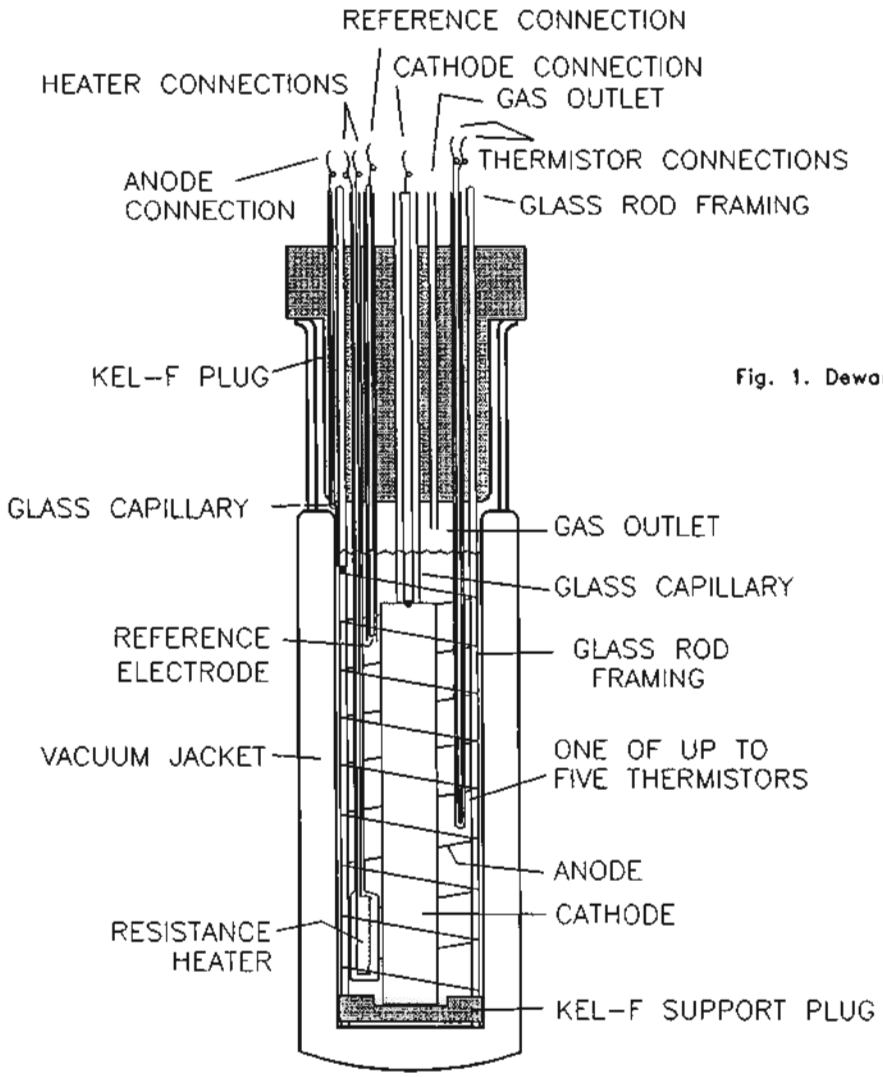

Fig. 1. Dewar calorimeter cell used in this work.

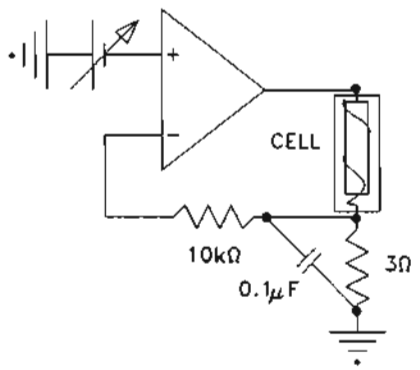

Fig. 2A. Schematic diagram of the feedback circuit used in this work for protection against galvanostat oscillations.

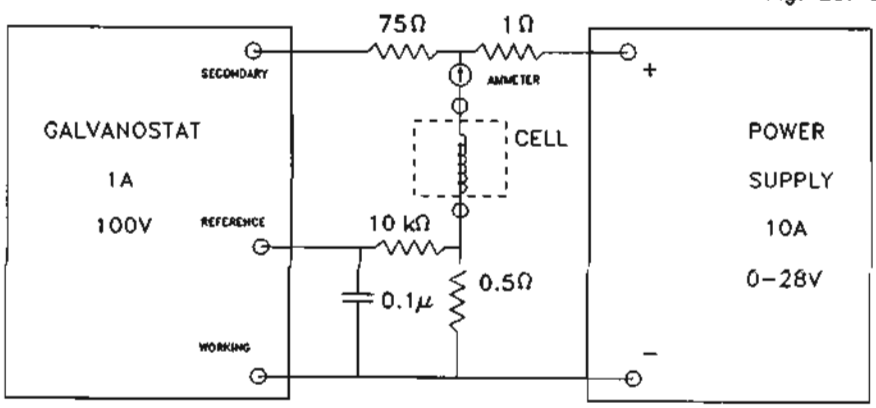

Fig. 2B. Schematic diagram of the circuit used in this work for high stabilization of a regulated power supply used as a high output current galvanostat.

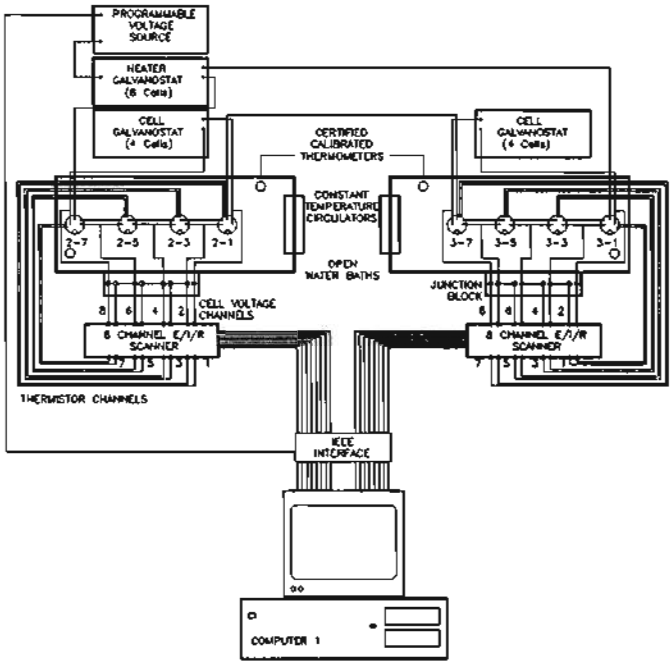

Fig. 3. Experimental layout for some of the calorimetric measurements reported in this paper.

A

ENTHALPY OF GAS STREAM $\gamma\frac{I}{F}\left\{\left[0.5C_{P,D_2} + 0.25C_{P,O_2} + 0.75\left(\frac{P}{P^\circ-P}\right)C_{P,D_2O,v}\right]\Delta\vartheta + 0.75\left(\frac{P}{P^\circ-P}\right)L\right\}$

$(E_{cell}(t) - \gamma E_{thermoneutral,cell})\, I \longrightarrow$

ENTHALPY INPUT TO THE CELL

$C_{P,D_2O,\ell}\left[M^0 - (1+\beta)\frac{\gamma It}{2F}\right]\frac{d\Delta\vartheta}{dt} - (1+\beta)\frac{\gamma I}{2F}C_{P,D_2O,\ell}\Delta\vartheta$

$\longrightarrow$ Radiation and Conduction $\longrightarrow$ HEAT LOSS FROM THE CELL

EXCESS ENTHALPY Q_f

CALIBRATION PULSE $+\Delta Q\, H(t-t_1)$ $-\Delta Q\, H(t-t_2)$

$\gamma\frac{I}{F}\int_0^t\left[0.5+0.75\frac{P}{P^\circ-P}\right]C_{P,D_2O,\ell}\Delta\vartheta'\,dt$

ENTHALPY OF MAKE-UP STREAM

B

$(E_{cell}(t) - E_{thermoneutral,bath})\, I \longrightarrow$

$C_{P,D_2O,\ell}\left[M^0 - (1+\beta)\frac{It}{2F}\right]\frac{d\Delta\vartheta}{dt} - \frac{\beta I}{2F}C_{P,D_2O,\ell}\Delta\vartheta$

$\longrightarrow$ Radiation and Conduction

Q_f $+\Delta Q\, H(t-t_1)$ $-\Delta Q\, H(t-t_2)$

$\frac{I}{F}\int_0^t\left[0.5+0.75\frac{P}{P^\circ-P}\right]C_{P,D_2O,\ell}\Delta\vartheta'\,dt$

Fig. 4. The full (A) and the approximate (B) "black box" models of the calorimeter shown in Fig. 1.

electrolysis. The nature of the enthalpy flows into and out of the "black box" will be explained by the following comments:

a) the enthalpy flow into the cell due to the electrical input is $(E_{cell}(t) - \gamma E_{thermoneutral,cell})I$. The term $E_{thermoneutral,cell}$ is the cell voltage at which the electrolysis is thermoneutral; this differs from the reversible potential of the reaction

$$2D_2 + O_2 \rightleftarrows 2D_2O$$

since the electrolysis takes place with an increase of entropy.

b) the current efficiency, γ, can be taken as unity (see Section 1).

c) in the analysis of the data we have neglected the enthalpy content of the gas stream due to the D_2O content, $0.75\left(\frac{P}{P^* - P}\right)C_{P,D_2O,v}\,\Delta\theta$, as well as that due to the evaporation of D_2O, $0.75\left(\frac{P}{P^* - P}\right)L$. Both these terms have been written assuming the gas stream is saturated with D_2O at the relevant cell temperature. The neglect of these terms causes an underestimate of the excess enthalpy. The terms are relatively small for values of $\Delta\theta < 20^{\circ}$ but the second, especially, becomes large and the dominant form of heat transfer from the cell as the temperature reaches the boiling point (See Section 4). Our calorimeters are unsuitable for measuring the heat outputs from the cells under these conditions.

There is a further term (not shown in Fig. 4A) which causes an additional underestimate of the excess enthalpy. This is due to the change in composition of the Pd-D electrode due to the increase of $\Delta\theta$ with time (see Fig.5). The dissolution of D in Pd is exothermic under the operating conditions so that a decrease of the D content with increasing $\Delta\theta$ will cause an absorption of heat in the cell. This effect is difficult to quantify since equilibrium cannot be maintained on the timescales of the measurement cycles. We have therefore neglected this term.

d) heat transfer from the calorimeter to the surroundings can be written in a variety of ways depending on its design and properties as well as the chosen level of approximation[3]. For the Dewar-type cells, Fig. 1, heat transfer for a hypothetical steady state generation of Q watts is controlled by a mixture of radiation and conduction

$$Q = k_R\left[\left(\theta_{bath} + \Delta\theta\right)^4 - \theta_{bath}^4\right] + k_C\Delta\theta \qquad (1)$$

Similarly for the steady state following the additional injection of ΔQ watts to calibrate the system we have

$$Q + \Delta Q = k_R\left[\left(\theta_{bath} + \Delta\theta + \Delta\Delta\theta\right)^4 - \theta_{bath}^4\right] + k_C\left[\Delta\theta + \Delta\Delta\theta\right] \qquad (2)$$

The separate determination of k_R and k_C leads to an increase in the random errors in the estimation of the heat flows from the cells. We have therefore adopted the strategy of neglecting the conductive term while making an appropriate increase in the radiative term

$$Q \cong k_R'\left[\left(\theta_{bath} + \Delta\theta\right)^4 - \theta_{bath}^4\right] \qquad (3)$$

and

$$Q \cong k_R'\left[\left(\theta_{bath} + \Delta\theta + \Delta\Delta\theta\right)^4 - \left(\theta_{bath} + \Delta\theta\right)^4\right] \qquad (4)$$

We have shown elsewhere[3] that this leads to a small systematic underestimate of the heat flow from the cell (and hence the excess enthalpy). However, as the correct value of the radiative term can be estimated from the Stefan-Boltzmann constant and the surface areas of the cells, a correction can readily applied (if this is desired) to give the heat output from the cells to within 1% of the enthalpy input or 1 milliwatt whichever is the greater. (for further comments on the application of equations (1) - (4) see Section 3. An important aspect of the approximations (3) and (4) is that any other term linear in $\Delta\theta$ can similarly be accounted for by making an appropriate increase or decrease in k_R (see Section 3).

A further factor which needs to be taken into account is that for a continuously reacting chemical system (open system) such as the electrochemical Dewar cells, the cell contents change with time. The extent of the radiant surface decreases with time while the length of any parallel conduction path increases with time. To a first approximation we

would therefore expect the heat transfer coefficients to decrease linearly with time and we write

$$Q \cong k_R'^0\left[1-\frac{(1+\lambda)\,\gamma It}{2FM^0}\right]\cdot \left[\left(\theta_{bath}+\Delta\theta\right)^4-\theta_{bath}^4\right] \qquad (5)$$

where the term λ allows for a more rapid decrease of the radiant surface area (and increase of the length of the conduction path) than would be predicted by electrolysis alone in view of the internal solid cell components. The superscript ^{0} here and elsewhere in this text denotes a value at a chosen time origin.

e) a general expression for the water equivalent is

$$M = M^0-\frac{(1+\beta)\,\gamma It}{2F} \qquad (6)$$

where, as for the heat transfer coefficient, the term β allows for a more rapid decrease of M with time than would be predicted by electrolysis alone. We expect $\beta < \lambda$.

f) the term $\frac{\gamma I}{F}\int_0^t\left[0.5+0.75\left(\frac{P}{P^*-P}\right)\right]\cdot C_{P,D_2O,\ell}\Delta\theta'\,dt$ is the enthalpy input to the cell due to the addition of D_2O to make up for the losses due to,electrolysis and evaporation. Here $\Delta\theta$ is the difference in temperature between the cell and make-up stream. In practice it has been found convenient to add D_2O at fixed intervals of time and, provided measurements are initiated at times longer than 6 thermal relaxation times following this addition, the effect of this term can be neglected in the further analysis.

We therefore obtain the differential equation governing the behavior of the calorimeter

$$C_{P,D_2O,\ell}\left[M^0-\frac{(1+\beta)\,\gamma It}{2F}\right]\frac{d\Delta\theta}{dt} - C_{P,D_2O,\ell}\frac{(1+\beta)\,\gamma I\Delta\theta}{2F} = -\left(E_{cell}(t)-\gamma E_{thermoneutral,cell}\right)I + Q_f(t) + \Delta QH(t-t_1) - \Delta QH(t-t_2)$$

$$-\frac{\gamma I}{F}\left\{\left[0.5C_{P,D_2}+0.25C_{P,O_2}+0.75\left(\frac{P}{P^*-P}\right)C_{P,D_2O,v}\right]\Delta\theta+0.75\left(\frac{P}{P^*-P}\right)L\right\} - k_R'^0\left[1-\frac{(1+\lambda)It}{2FM^0}\right]\cdot\left[\left(\theta_{bath}+\Delta\theta\right)^4-\theta_{bath}^4\right] \qquad (7)$$

Equation (7) is difficult to apply because $E_{cell}(t)$ and $Q_f(t)$ are unknown functions of time. We note, however, that since we are only concerned with small changes of temperature at any given origin, θ^0, we can carry out a Taylor series expansion at this point and, retaining only the first derivatives we obtain

$$\left\{\frac{dE_{cell}}{d\theta}+\frac{d}{d\theta}\left[\frac{0.75I}{F}\left(\frac{P}{P^*-P}\right)\cdot\left(C_{P,D_2O,v}\,\Delta\theta+L\right)\right]\right\}I\Delta\theta' - \frac{\psi I}{\theta^0}\Delta\theta' \qquad (8)$$

where $\Delta\theta' = \Delta\theta - \Delta\theta^0$ (see Glossary). We assume also that Q(t) is constant during any one measurement cycle and, taking note also of

$$\Delta H^{\circ}_{cell} = \Delta H^{\circ}_{bath} + \sum_i \nu_i C_{P,i}\Delta\theta \qquad (9)$$

as well as of b) and c) we can write (7) in the more tractable form

$$C_{P,D_2O,\ell}\left[M^0-\frac{(1+\beta)It}{2F}\right]\frac{d\Delta\theta}{dt} - C_{P,D_2O,\ell}\frac{\beta I\Delta\theta}{2F} = -\left(E^0_{cell}-E_{thermoneutral,bath}+\frac{\psi\Delta\theta'}{\theta^0}\right)I + Q_f(t) + \Delta QH(t-t_1) - \Delta QH(t-t_2)$$

$$- k_R'^0\left[1- \frac{(1 + \lambda)It}{2FM^0}\right]\cdot$$

$$\left[\left(\theta_{bath}+ \Delta\theta\right)^4 - \theta^4_{bath}\right] \qquad (10)$$

This equation describes the modified "black-box" shown in Fig. 4B.

Section 3

Data Evaluation and Error Analysis

As is well understood in the field of chemical kinetics, it is necessary to fit the integrated form of equation (10) to the experimental data in order to extract the parameters of the equations; application of such equations at a single point leads to erroneous results. It is naturally not possible to derive an analytical solution to (10) since this equation is non-linear and inhomogeneous. An approximate solution, however, can be obtained[3] using the linearized form of the heat transfer term $4k_R'^0\theta^3_{bath}\left[1 - \frac{(1 + \lambda)It}{2FM^0}\right]\Delta\theta$ and this solution shows that the heat transfer coefficient to be used in the evaluation of Q_f at a given point is $\left[4k_R'^0\theta^3_{bath} - \frac{\psi I}{\theta^0}\right]\left[1 - \frac{(1 + \lambda)It}{2FM^0}\right]$ rather than the value $4k_R'^0\theta^3_{bath}\left[1- \frac{(1 + \lambda)It}{2FM^0}\right]$ which would be predicted from the thermal balance at a single point and it is the former rather than the latter value which has to be used in determining the thermal output of the cell in applying the linearized equations.[3]

These linearized equations can be shown to be in close accord with the experimental data for small values of $\Delta\theta$ but these equations will naturally not be applicable for large values of $\Delta\theta$ say, $>10^{0}$.[3] In order to obtain approximate values of Q, $k_R'^0\left[1 - \frac{(1 + \lambda)It}{2FM^0}\right]$, and Q_f we have therefore applied the calculation scheme illustrated in Fig. 5A and using equations (3) and (4). Fig. 5B illustrates a set of such calibration pulses determined during one measurement cycle and Fig. 5C illustrates the time dependence of the derived heat transfer coefficients. It can be seen that there is a systematic error due entirely to the uncertainty in the refilling of the Dewars at the beginning of any one measurement cycle. Superposition of the plots at the mid-point (27 hours after addition of the D_2O) shows that the standard deviation of the remaining 132 points in 33 experimental series is only 0.15%, a value which is roughly in line with the errors in measurement of the absolute temperatures in (3) and (4). These data show that it is essential to calibrate the cells for each desired measurement of the thermal output.

Nevertheless, such determinations are evidently approximate not only because of the underestimate of k_R' (see Section 2d) but also because of the assumption that Q is unchanged in applying the heater calibration pulse is strictly speaking not valid (see the decrease in E_{cell}) with t during the heater calibration period $t_1 < t < t_2$, Fig. 5A). Accurate values of Q can only be obtained by fitting the whole of the transient predicted from (10) (or any other chosen representation of the calorimeter)to the experimental data and making the estimate of Q and hence Q_f at the point designated ^{0} (where the term $\frac{\psi\Delta\theta'}{\theta^0}$ is zero) Such a fitting procedure must be carried out in an unbiased manner. We have used non-linear regression and, in this, have used the simplest forward integration method

$$\Delta\theta_{n+1} = \Delta\theta_n + \left(\frac{d\Delta\theta}{dt}\right)_n \Delta t \qquad (11)$$

and we have used the parameters Q, $k_R'^0$, Q_f and $(1 + \lambda)$ estimated according to Figs. 5A and 5B as starting values for the regression procedures. The parameter ψ has been estimated from the E_{cell} - t plot using linear regression. In this way the number of parameters to be fitted to (10) has been reduced from 5 to 4 thereby speeding the calculation. In view of the curvature of the parameter space hypersurfaces, it has also been found to be convenient to regard

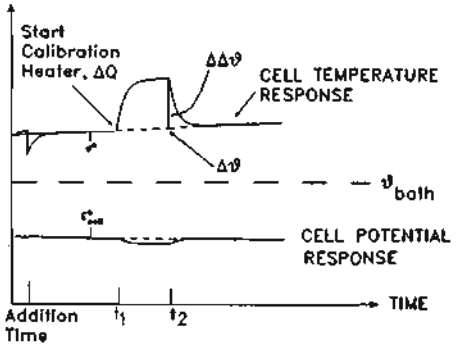

Fig. 5A. Schematic diagram for the experimental determination of approximate heat flow in the calorimeter. The response shows the application of the calibration pulse of strength ΔQ which leads to an eventual new sloping steady state temperature $\Delta\Delta\vartheta$ degrees above the linearly sloping baseline temperature. Calculation of the output heat flow at this level of approximation requires simply the measurement of the three temperatures indicated and the magnitude (ΔQ) of the calibration heater pulse. In applying equation (10) it is convenient to set the origin $t = 0$ at ~6 thermal relaxation times following the addition of D_2O to make up for losses due to electrolysis and evaporation. At this point $\vartheta = \vartheta^o$ $E_{cell} = E^o_{cell}$, $k'_R = k'^o_R$, and $M = M^o$.

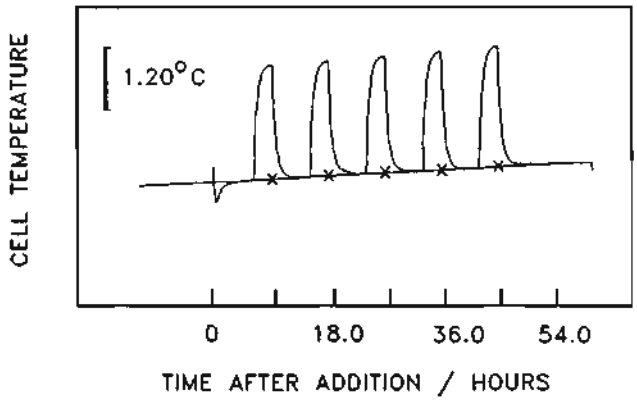

Fig. 5B. Typical set of heat flow calibration cycles made at 9, 18, 27, 36, and 45 hours after addition of D_2O. for a 0.1 x 10 cm Pd electrode in 0.1MLiOD. The current density was 64 mA cm^{-2}. x = calculated baseline.

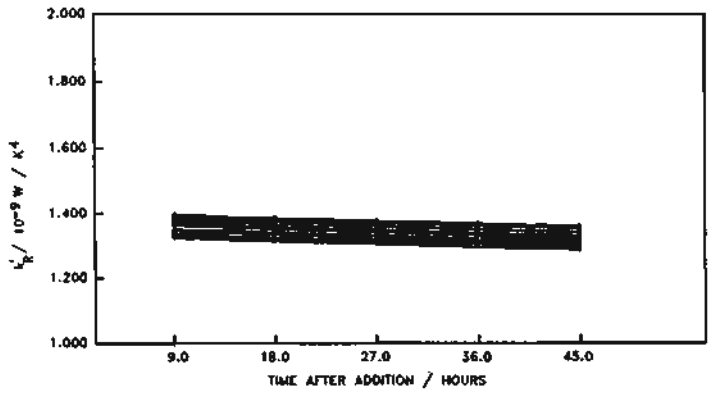

Fig. 5C. 165 derived heat transfer coefficients for 33 sets of calibration cycles for a typical cell, showing the effect of the systematic error discussed in the text.

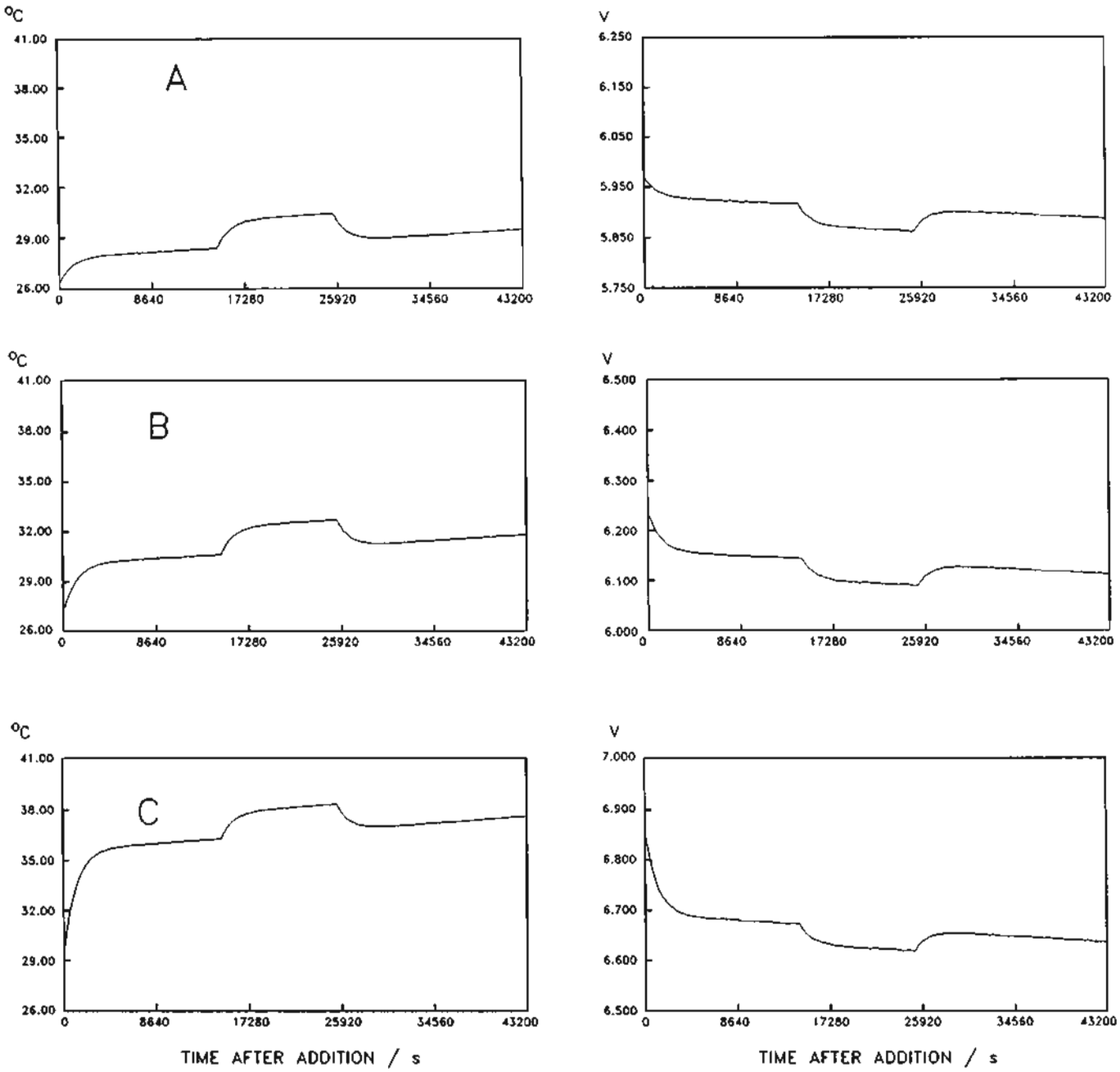

Fig. 6A. Temperature °C above bath vs. time (left plot) and cell potential (V) vs. time (lower right) data for a 0.4 x 10 cm Pd rod in 0.1M LiOD solution. The applied current was 800 mA, the bath temperature was 29.87°C, and the estimated Q_f was 0.158 W. The time of the measurement was approximately 0.45 x 10^6s after the beginning of the experiment.

Fig. 6B. Same as Fig. 6A except time of measurement approximately 0.89 x 10^6s. Estimated Q_f = 0.178 W.

Fig. 6C. Same as Fig. 6A except time of measurement approximately 1.32 x 10^6s. Estimated Q_f = 0.372 W.

$$\frac{\left(E^0_{cell} - E_{thermoneutral,bath} \right) I + Q_f}{C_{P,D_2O,\ell}\, M^0}$$

as one of the free parameters of the calculation.

We have used a Marquardt-type algorithm for the fitting procedure and it should be noted that the diagonal elements of the error matrix derived in this calculation (the inverse of the matrix used in the parameter estimation) directly give the standard deviation of the parameters. In this way we have shown that the parameter

$$\frac{\left(E^0_{cell} - E_{thermoneutral,bath} \right) I + Q_f}{C_{P,D_2O,\ell}\, M^0}$$

can be estimated to ±0.1% throughout the operating range. This is also the error of $\left(E^0_{cell} - E_{thermoneutral,bath}\right) I + Q_f$ since the independently derived value of M^0 has errors of ≅ ±0.01%. Even higher precisions could well be achieved by using a larger number of calibration pulses but we have not done this so far in our work as we have only estimated $\left(E^0_{cell} - E_{thermoneutral,bath}\right) I$ to ≅ 0.1% (the error of this quantity is controlled by σ_I). This error must be added to that of $\left(E^0_{cell} - E_{thermoneutral,bath}\right) I + Q_f$ to obtain the total error of the excess enthalpy listed in Tables 1 and 2.

Section 4
Results

An example of a set of temperature - time and the associated potential - time plots is illustrated for one experiment at three different times in Figs. 6A-C. Fig. 7 illustrates the degree of fit which can be obtained by using the non-linear regression procedure outlined in the previous section and Tables 1 and 2 illustrate the results of measurements of the excess enthalpy using both the approximate and exact methods of data analysis. We have also included some data taken prior to our first publication [1,2] which were obtained using only the approximate method of data analysis.

The marked excess enthalpy production on 0.1 and 0.2 and 0.4 cm diameter electrodes, (Table 1) must be viewed in terms of the slightly negative excess enthalpies for the blank experiments, Table 2.[1] This slightly negative value is due to the method of calculation which underestimates the heat output from the cell (see Section 2D). In many ways we regard the "zero" result on 0.8 cm diameter electrodes as the most significant blank as it shows that almost exact thermal balances can be obtained using our methodology for systems identical to those giving marked excess enthalpy. The differences between the 0.1, 0.2, 0.4 and the 0.8 cm electrodes also point to the importance of the metallurgical procedures in devising electrodes showing excess enthalpy generation.

Section 5
Discussion

It can be seen that many (perhaps all?) of the assertions e.g.[5,10-16] which have been made about our experiments are erroneous. We would stress here that it is perfectly possible to obtain accurate values of the heat output from the cells and, hence, the excess enthalpy provided due attention is paid to the design of the calorimeters and control of the environment and providing modern methods of data analysis are used. We would also stress the importance of deriving error estimates from a single experiment rather than from the variation of a parameter (here the excess enthalpy) from a set of experiments as the variability of the parameter may itself be a key feature of the phenomenon to be observed. In this context it is of interest that the variability of the results at low to intermediate current densities (which have been widely used in attempts to replicate our work) is large and far in excess of the errors of each individual experiment. This variability may point to the importance of the precise nature of the surface conditions and/or history of the

---

[1] Much of this data was available at the time of our first publication but the Editor of Nature refused to publish a letter to correct the many erroneous statements which had been made in the Editorials of the Journal.

Table 1. Excess enthalpy observed for 0.1, 0.2, and 0.4 cm diameter palladium rods as a function of current density and electrolyte composition.

Rod Dia.[a] /cm	Electrolyte[b]	Current Density /mA cm^{-2}	E_{cell} /V	Q_{input} /W	Q_{excess} /W	Approximate Specific Q_{excess} /W cm^{-3}	Specific Q_{excess} From Regression Analysis /W cm^{-3}	
0.1	$\mathcal{D}$	64	3.637	0.419	0.042	0.53	0.581	±0.003
0.1*	$\mathcal{S}$	64	2.811	0.032	0.001	0.140	0.1442	±0.0002
0.1	$\mathcal{D}$	128	4.000	0.984	0.160	2.04	2.043	±0.003
0.1*	$\mathcal{S}$	128	3.325	0.089	0.005	0.486	0.5131	±0.0006
0.1	$\mathcal{D}$	256	5.201	2.93	0.313	3.99	4.078	±0.007
0.1*	$\mathcal{D}$	512	9.08	1.51	0.17	17.3	18.19	±0.02
0.1	$\mathcal{D}$	512	6.085	7.27	1.05	13.4	13.77	±0.02
0.1*	$\mathcal{D}$	1024	11.640	4.04	1.03	105.	112.8	±0.1
0.2	$\mathcal{D}$	64	4.139	1.040	0.123	0.39	0.419	±0.003
0.2	$\mathcal{S}$	64	4.780	1.30	0.006	0.019	0.021	±0.001
0.2	$\mathcal{M}$	64	3.930	0.956	0.024	0.077	0.077	±0.001
0.2	$\mathcal{D}$	128	8.438	5.52	1.65	5.25	5.68	±0.01
0.2*	$\mathcal{S}$	128	4.044	0.250	0.028	0.713	0.714	±0.001
0.2*	$\mathcal{M}$	256	6.032	0.898	0.056	1.42	1.498	±0.002
0.2*	$\mathcal{D}$	512	8.25	2.68	0.66	16.8	17.02	±0.04
0.2*	$\mathcal{M}$	512	9.042	3.00	0.603	15.3	16.03	±0.01
0.2*	$\mathcal{S}$	1024	7.953	5.13	2.80	71.2	75.42	±0.08
0.4	$\mathcal{D}$	64	5.137	2.88	0.502	0.40	0.411	±0.001
0.4	$\mathcal{D}$	64	5.419	3.10	0.263	0.209	0.214	±0.003
0.4**	$\mathcal{D}$	64	4.745	2.24	0.117	0.106	0.145	±0.002
0.4*	$\mathcal{M}$	64	3.519	0.198	0.0005	0.002	0.0023	±0.0002
0.4	$\mathcal{D}$	128	6.852	8.50	1.05	0.84	0.842	±0.009
0.4*	$\mathcal{D}$	256	7.502	2.38	0.311	1.98	1.999	±0.003
0.4*	$\mathcal{D}$	512	8.66	5.70	2.18	13.9	14.41	±0.05
0.4*	$\mathcal{D}$	512	10.580	7.23	1.65	10.5	11.09	±0.02

(a) All rod lengths 10cm or *1.25cm or **8.75cm

(b) $\mathcal{D}$: 0.1M LiOD; $\mathcal{S}$: 0.50M Li_2SO_4; $\mathcal{M}$: 0.1M LiOD + 0.45M Li_2SO_4. All measurements were made in the same batch of D_2O of 99.9% isotopic purity. Measurements using electrolytes labelled $\mathcal{S}$ and $\mathcal{M}$ have been made since 23rd March, 1989.

Table 2. Results for blank experiments on platinum and palladium rods as a function of current density and electrolyte composition.

Rod Dia.[a]	Electrolyte[c]	Current Density	E_{cell}	Q_{input}	Q_{excess}	Approximate Specific Q_{excess}	Specific Q_{excess} From Regression Analysis	
/cm		/mA cm^{-2}	/V	/W	/W	/W cm^{-3}	/W cm^{-3}	
Palladium Electrodes:								
0.1	*W*	32	3.605	0.212	-0.001	-0.009	-0.0097	±0.0002
0.1	*W*	64	3.873	0.479	-0.001	-0.014	-0.0165	±0.0005
0.1[d]	*W*	128	5.186	1.482	-0.001	-0.001		
0.1[d]	*W*	256	8.894	5.931	-0.001	-0.007		
0.1	*W*	512	11.29	15.70	-0.001	-0.008	-0.01	±0.02
bd[b]	*D*	0.8	2.604	1.458	-0.001	-0.000		
0.8[d]	*D*	8	3.365	0.365	-0.001	-0.000		
0.8[d]	*D*	8	3.527	0.397	-0.003	-0.000		
Platinum Electrodes:								
0.1[d]	*D*	64	3.800	0.452	0.000	0.000		
0.1[d]	*D*	64	4.138	0.520	-0.001	-0.008		
0.1[d]	*D*	256	6.218	3.742	-0.001	-0.028		
0.1	*W*	64	4.602	0.624	-0.002	-0.023	-0.0232	±0.0006
0.1	*W*	64	4.821	0.668	-0.003	-0.038	-0.0392	±0.0006
0.1	*W*	512	12.02	16.86	-0.001	-0.007	-0.01	±0.02

(a) All rod lengths 10cm.
(b) Palladium sheet electrode 8 x 8 x 0.2cm.
(c) *D*: 0.1M LiOD; *W*: 0.1M LiOH; All measurements in D_2O were made in the same batch as that used in the experiments in Table 1.
(d) Data available March 23, 1989. These data were evaluated by another method and not by those described in this paper.

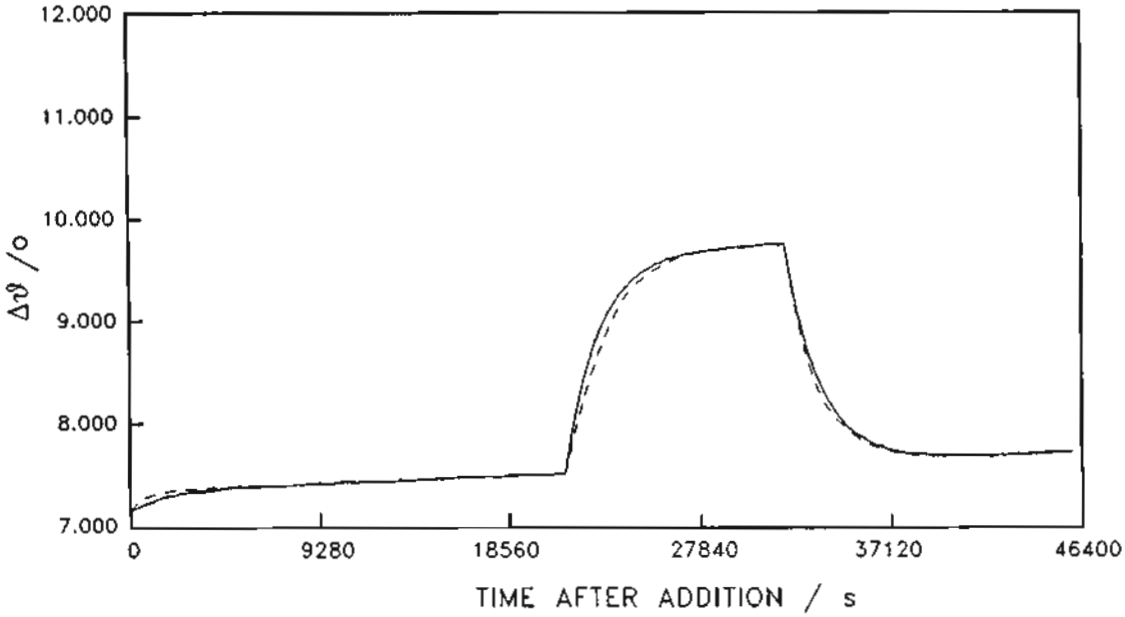

Fig. 7. Figure showing the degree of fit of the "black box" model in Fig. 4B to actual experimental data from an experiment using a 0.2 x 10cm Pd rod cathode in 0.1MLiOD. The dotted line in the figure represents the fit obtained using estimated values of the several cell parameters and was obtained by the forward integration technique described in the text to force the fit of the data to the model at the starting point (t = 0), the point of application of the calibration heater pulse, the point at the end of the calibration heater pulse, and the point at the end of the experiment. The solid line (which in this figure is coincident with the experimental data) is the fit obtained to the model by the Marquardt algorithm for the non-linear regression technique described in the text.

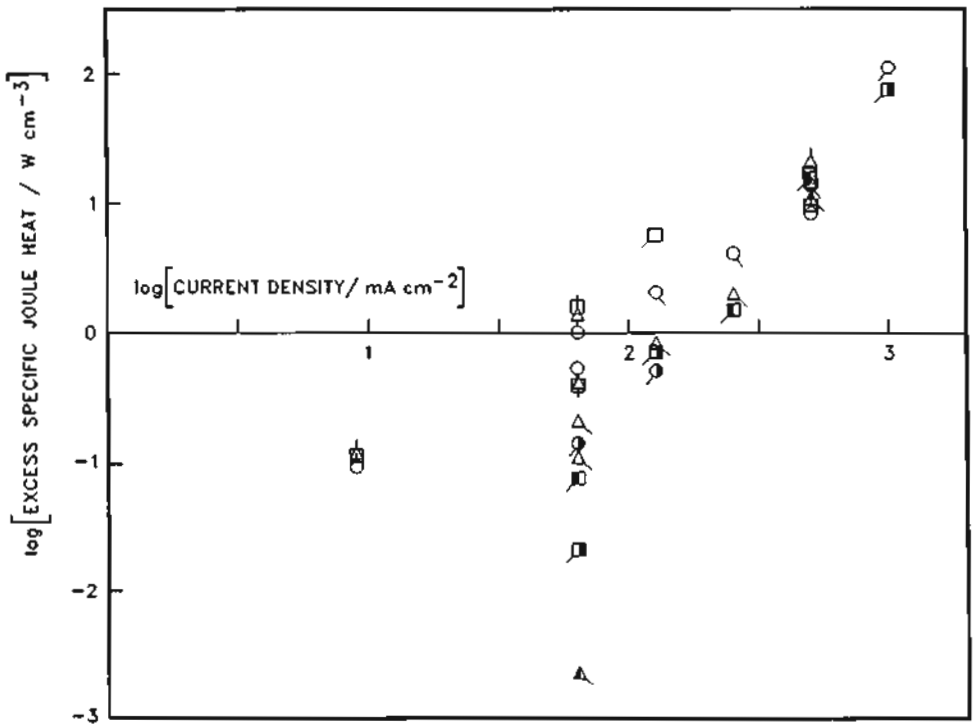

Fig. 8. Log-log plot (Excess enthalpy vs. current density) for a group of typical calorimetric experiments using Pd electrodes in D_2O electrolytes.

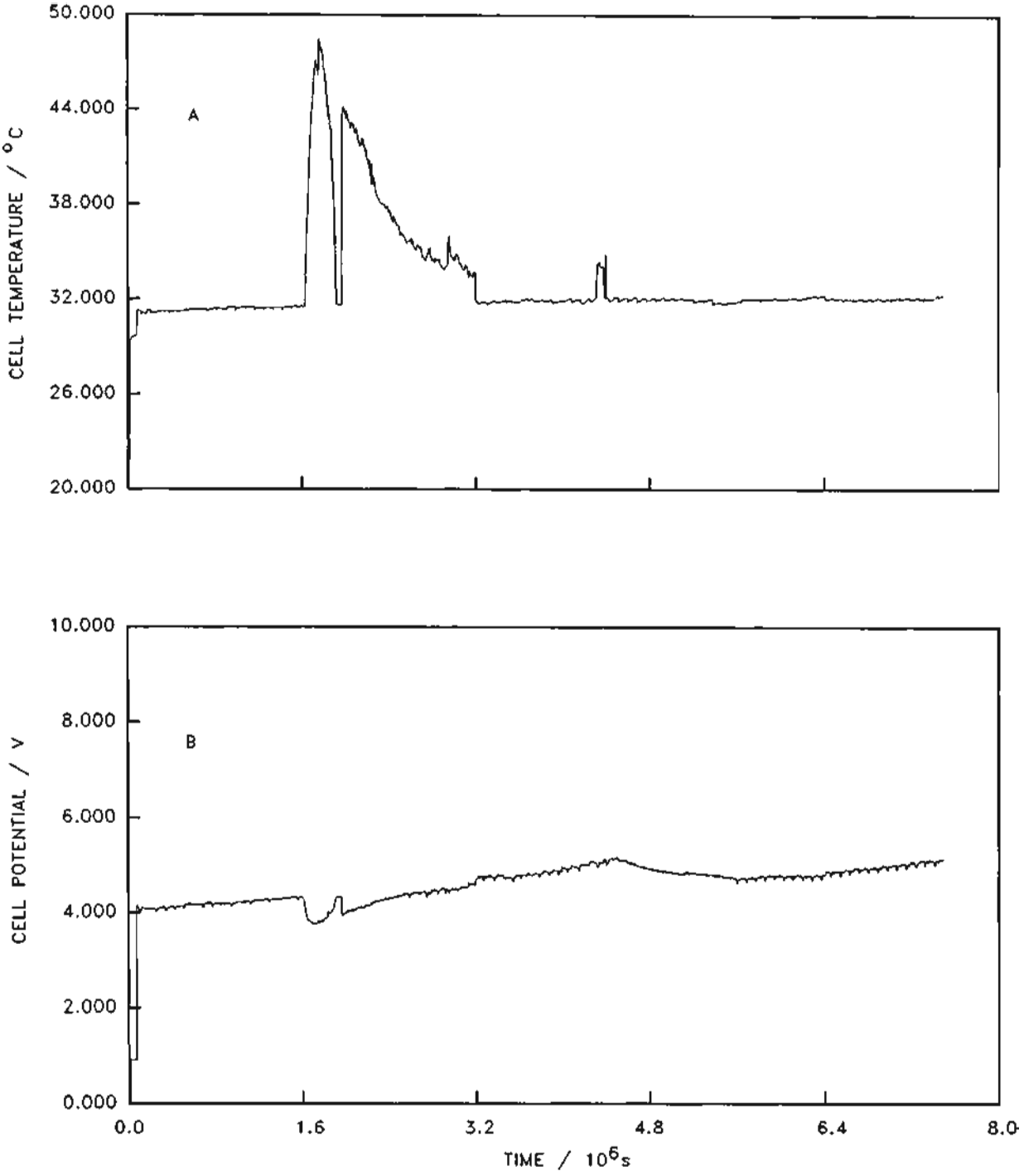

Fig. 9A. Demonstration of a "burst" of excess enthalpy for a long period of time. The upper plot is the cell temperature vs. time and the lower plot is the cell potential vs. time. The electrode was a 0.4 x 1.25 cm Pd rod in 0.1M LiOD solution. The current density was 64 mA cm^{-2}, and the bath temperature was held at 29.87°C.

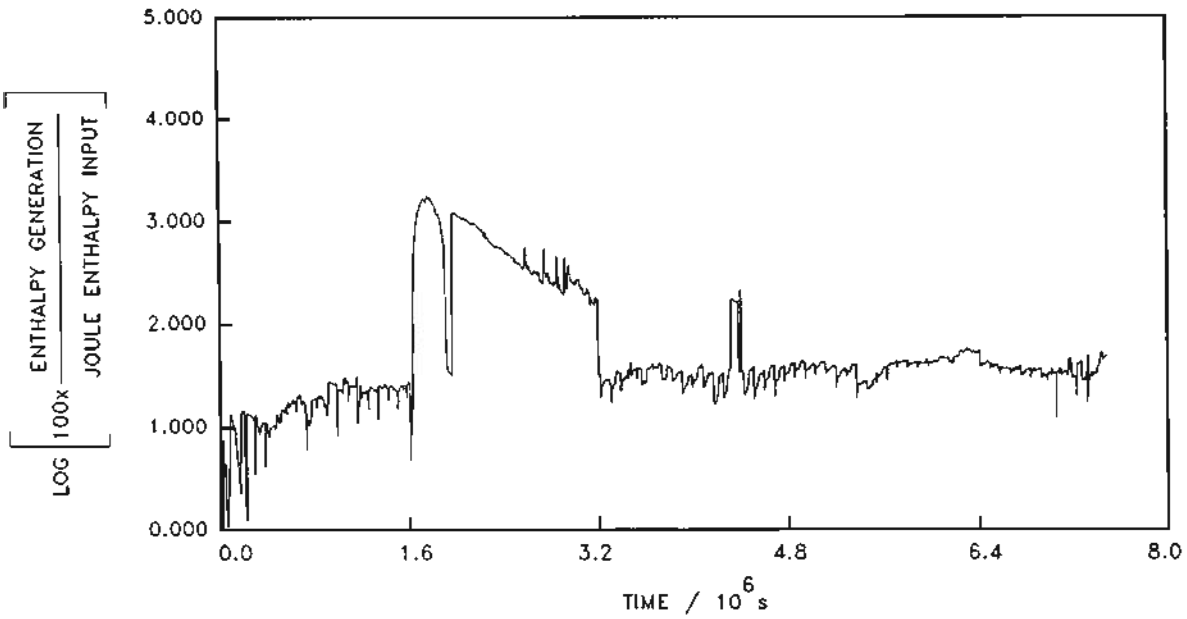

Fig. 9B. Figure showing the calculated rate of excess enthalpy generation as a function of time for Fig. 9A, and

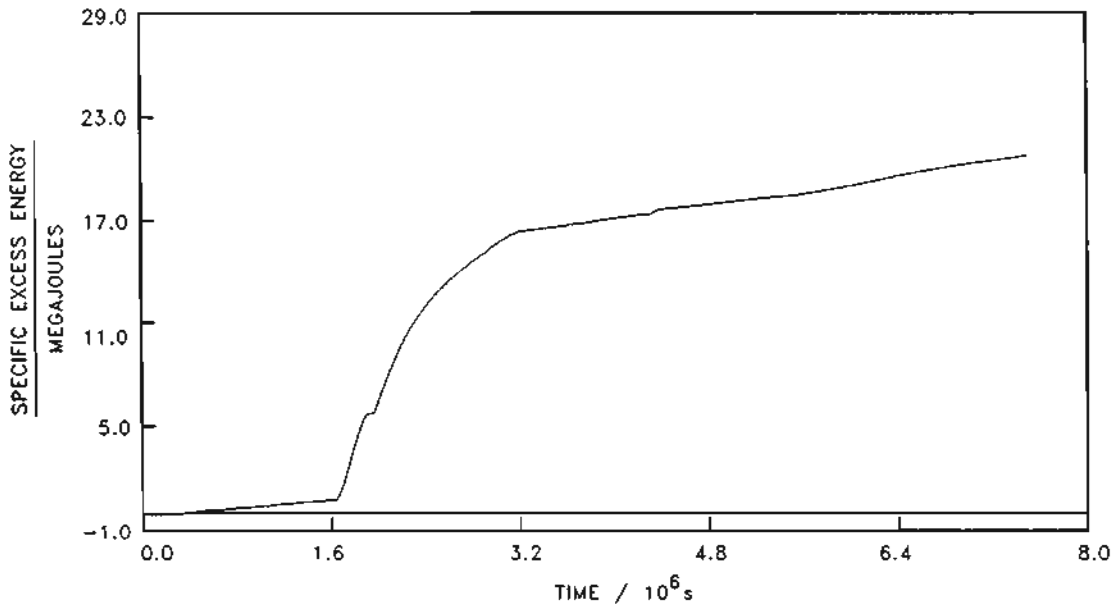

Fig. 9C. Figure showing the total specific excess energy output as a function of time for this cell.

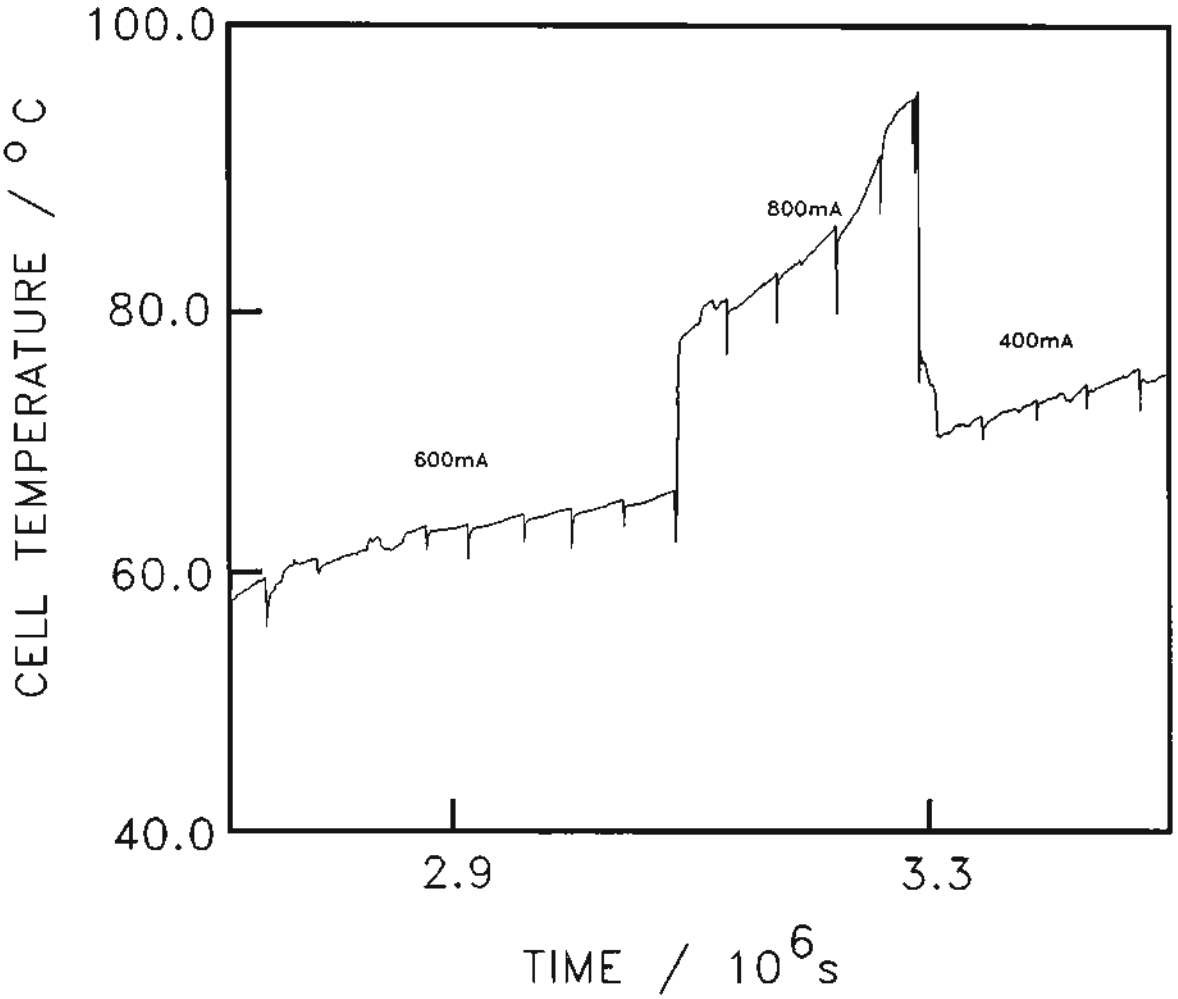

Fig. 10. A cell temperature vs. time plot for a 0.4 x 1.25 cm palladium rod electrode in 0.1M LiOD for a period during which the cell contents went to the boiling point.

electrodes in defining the phenomenon.

It can be seen that the excess enthalpies increase markedly with the current density so much so that the results have the appearance of a threshold phenomenon. However, experiments of very high precision at low current densities are required before this can be confirmed. On balance we still believe that the results confirm that excess heat generation is a bulk phenomenon, Fig. 8, although this cannot now be stated as firmly as it appeared from the results available in the spring of 1989. The levels of enthalpy generation during the duration of a typical experiment (3 months) are such (hundreds of Megajoules cm^{-3}) that they must be attributed to nuclear processes. In particular, it is inconceivable that chemical or non-nuclear physical energy could be stored in the system at these levels and then be released over prolonged periods of time[17]. The phenomenon of "bursts" in the enthalpy production which we first described[18] shortly after the publication of our preliminary paper[1] is also of interest in this context. Figs. 9A, B and C illustrate the $\Delta\theta$ - t , the specific excess enthalpy - t and the cumulative specific enthalpy - t data for the largest "burst" we have observed to date. The total specific excess over the period of the "burst" ($\cong$16 MJ cm^{-3} over 16 days) is again of such a magnitude that the heat release can only be attributed to nuclear processes. The heat output during this burst was 17 times (average value) and 40 times (peak value) of the enthalpy input. In some cells e.g. Fig. 10, the temperature rises rapidly to boiling. When this occurs, it is difficult to accurately measure the heat flows (see Section 2c above). The heat output, however, must be extremely high.

Our current work is concentrated on the design and implementation of factorial experiments in which we are seeking to define more closely the effects of the many variables which control the excess enthalpy. The instrumentation and procedures which we are using in the execution of these experiments are essentially the same as those described in this paper.

ACKNOWLEDGEMENTS

We thank the Office of Naval Research and the University of Utah for support of this work. All of the special grade electrodes used in this work were lent to us by Johnson-Matthey PLC, to whom we are indebted.

REFERENCES

[1] M. Fleischmann, S. Pons, and M. Hawkins, J. Electroanal Chem. 261 (1989) 301.

[2] M. Fleischmann, S. Pons, and M. Hawkins, J. Electroanal Chem. 263 (1989) 187.

[3] M. Fleischmann, S. Pons, M. Anderson, L. J. Li, and M. Hawkins, J. Electroanal. Chem., in the press.

[4] O. Levenspiel, "Chemical Reaction Engineering", J. Wiley & Sons, New York, 1972.

[5] N. Lewis, M. J. Heben, A. Kumar, S. R. Lunt, G. E. McManis, G. M. Miskelly, R. M. Penner, M. J. Sailor, P. G. Santangelo, G. A. Shreve, B. J. Tufts, M. G. Youngquist, C. A. Barnes, R. W. Kavanagh, S. E. Kellog, R. B. Vogelaar, T. R. Wang, R. Kondrat, and R. New, Nature340 (1989) 525, and 175th Meeting of the Electrochemical Society, Los Angeles, CA USA May, 1989.

[6] S. Pons and M. Fleischmann, J. Fusion Technology, in the press.

[7] G. Kreysa, G. Marx, and W. Plieth, J. Electroanal. Chem. 266 (1989) 437.

[8] V. J. Cunnane, R. A. Scannel, and D. J. Schiffrin, J. Electroanal. Chem. 269 (1989) 437. .

[9] L. L. Zahm, A. C. Klein, S. E. Binney, J. N. Reyes, Jr., J. F. Higgenbotham, A. H. Robinson, and M. Daniels, J. Electroanal. Chem., submitted.

[10] D. E. Williams, D. J. S. Findlay, D. H. Craston, M. R. Sené, M. Bailey, S. Croft, B. W. Hooten, C. P. Jones, A. R. J. Kucernak, J. A. Mason, and R. I. Taylor, Nature 342 (1989) 375.

[11] M. Chemla, J. Chevalet, R. Bury, and M. Perie, Cold Fusion Session, 40th Meeting of the International Society of Electrochemistry, Kyoto, Japan, 11-18 September 11-18, 1989.

[12] A. Bruggeman, M. Loos, C. Van der Poorten, R. Craps, R. Leysen, F. Poortmans, G. Verstappen, and M. Snykers, Studiecentrum voor Kernenergie Report, September 1989.

[13] V. Eberhard, G. Fieg, K. Flory, W. Heeringa, H. V. Karow, H. O. Klages, J. Lebkücher, M. Möschke, C. Politis, J. Römer, H. Schnider, G. Völker, H. Werle, H. Würtz, and B. Zeitnitz, Report INR-1653 of the Kernforschungszentrum Karlsruhe, West Germany (1989).

[14] R. D. Armstrong, Session on Cold Fusion, 40th Meeting of the International Society of Electrochemistry, Kyoto, Japan, 17-22 September, 1989.

[15] H. S. Bosch, G. A. Wurden, J. Gernhardt, F. Karger, and J. Perchermeier, Report IPP III / 149' of the Max-Planck Institut für Plasmaphysik, Garching bei München, West Germany.

[16] G. Kreysa International Society of Electrochemistry, Kyoto, Japan, 17-22 September, 1989 and Meeting of the Electrochemical Society, Los Angeles, CA, USA May (1989).

[17] R. C. Kainthla, M. Sklarczyk, L. Kaba, G. H. Lin, O. Velev, N. J. C. Packham, J. C. Wass and J. O'M. Bockris, Inst. J. Hydrogen Energy, 14 (1989) 771.

[18] M. Fleischmann and S. Pons, Meeting of the Electrochemical Society, Los Angeles, CA, USA May (1989).

GLOSSARY OF SYMBOLS USED

$C_{P,D_2O,\ell}$ Heat capacity of liquid D_2O, $JK^{-1}mol^{-1}$.

$C_{P.D_2O,v}$ Heat capacity of D_2O vapor, $JK^{-1}mol^{-1}$.

$C_{P,i}$ Heat capacity of O_2, D_2, or $(D_2O)_\ell$, $JK^{-1}mol^{-1}$.

E_{cell} Measured cell potential, V.

$E_{cell,t=0}$ Measured cell potential time when the initial values of parameters are evaluated, V.

$E_{thermoneutral,bath}$ Potential equivalent of the enthalpy of reaction for the dissociation of heavy water at the bath temperature, V.

F Faraday constant, 96484.56 $C\ mol^{-1}$

H Heaviside unity function.

I Cell current, A.

k_C Heat transfer coefficient due to conduction, $W\ K^{-1}$.

k_R Heat transfer coefficient due to radiation, $W\ K^{-4}$.

k_R^0 Heat transfer coefficient due to radiation at a chosen time origin, $W\ K^{-4}$.

k_R' Effective heat transfer coefficient due to radiation, $W\ K^{-4}$.

$k_R'^0$ Effective heat transfer coefficient due to radiation at a chosen time origin, $W\ K^{-4}$.

ℓ Symbol for liquid phase.

L Enthalpy of evaporation, $J\ mol^{-1}$.

M Heavy water equivalent of the calorimeter, mols.

M^0 Heavy water equivalent of the calorimeter at a chosen time origin.

n Iteration number (data point number).

P Partial pressure, Pa.

P* Atmospheric pressure, Pa.

Q	Rate of steady state heat generation at a given temperature, W.
Q_f	Rate of generation of excess enthalpy, W.
t	Time, s.
β	Dimensionless term allowing for more rapid time dependent decrease of water equivalent of cell than that expected from electrolysis alone.
γ	Current efficiency of electrolysis toward a given reaction.
$\Delta H^{\varnothing}$	Standard free enthalpy change, J mol^{-1}.
ΔQ	Rate of heat dissipation of calibration heater, W.
$\Delta\theta$	Difference in cell and bath temperature at a given rate of enthalpy release, K.
$\Delta\theta^0$	Difference in temperature between the cell and the bath at a chosen time origin, K.
$\Delta\theta'$	Difference in cell and make-up temperature, K.
$\Delta\theta'$	$\Delta\theta - \Delta\theta^0$, K.
$\Delta\theta_n$	Difference in cell and bath temperature at the n^{th} time interval, K.
$\Delta\theta_{n,calc}$	Calculated difference in cell and bath temperature at the n^{th} time interval, K.
$\Delta\theta_{n,exp}$	Difference in experimental cell and bath temperature at the n^{th} time interval, K.
$\Delta\Delta\theta$	Temperature rise in cell due to application of a calibration pulse of heat, K.
θ_{bath}	Bath temperature, K.
λ	Dimensionless parameter determining the more rapid decrease of the radiant surface area than would be predicted by electrolysis alone.
ν_i	Stoichiometric coefficients.
σ_n	Sample standard deviation of a given temperature measurement, K.
χ^2	Sum of inverse variance weighted deviations between experimental data and values predicted by the model using the non-linear regression fitting algorithm.
ψ	Slope of the change of cell potential with temperature, V.